IEEE Access
Multidisciplinary | Rapid Review | Open Access Journal

Received 4 April 2023, accepted 1 May 2023, date of publication 5 May 2023, date of current version 19 May 2023.
Digital Object Identifier 10.1109/ACCESS.2023.3273529

RESEARCH ARTICLE

MBAHIL: Design of a Multimodal Hybrid Bioinspired Model for Augmentation of Hyperspectral Imagery via Iterative Learning for Continuous Efficiency Enhancements

DIPEN SAINI[1], RAHUL MALIK[1], RACHIT GARG[1], (Member, IEEE), MOHAMMAD KHALID IMAM RAHMANI[2], (Senior Member, IEEE), MD. EZAZ AHMED[2], DEEPAK PRASHAR[1], SUDAN JHA[3], (Senior Member, IEEE), JABEEN NAZEER[4], AND SULTAN AHMAD[4,5], (Member, IEEE)

[1]School of Computer Science and Engineering, Lovely Professional University, Phagwara, Punjab (India) - 144411
[2]College of Computing and Informatics, Saudi Electronic University, Riyadh 11673, Saudi Arabia
[3]Department of Computer Science and Engineering, School of Engineering, Kathmandu University, Banepa, Kathmandu 45200, Nepal
[4]Department of Computer Science, College of Computer Engineering and Sciences, Prince Sattam Bin Abdulaziz University, Al-Kharj 11942, Saudi Arabia
[5]Department of Computer Science and Engineering, University Center for Research and Development (UCRD), Chandigarh University, Mohali, Punjab 140413, India

Corresponding authors: Md. Ezaz Ahmed (m.ezaz@seu.edu.sa) and Sultan Ahmad (s.alisher@psau.edu.sa)

ABSTRACT The augmentation of hyperspectral images requires the design of high-density feature analysis & band-fusion models that can generate multimodal imagery from limited information sets. The feature analysis models use deep learning operations to maximize inter-class variance while minimizing inter-class variance levels for efficient classification operations. When combined with intelligent band-fusion methods, such models allow the augmentation model to enhance its classification efficiency under different use cases. Existing band-fusion-based augmentation models for hyperspectral images do not incorporate continuous efficiency enhancements and showcase higher complexity levels. Furthermore, these models can't be scaled for more varied use cases because their use is restricted to specific image types. To overcome these issues, we designed a novel multimodal hybrid bioinspired model for the augmentation of hyperspectral imagery via iterative learning for continuous efficiency enhancements. The proposed model initially represents input images into Fourier, Laplacian, Cosine, multimodal Wavelet, Mellin, and Z-Transform domains, which will assist in describing the images in multimodal domains. These transformed image sets are passed through a convolutional filter to extract windowed feature sets. A Grey Wolf Optimizer (GWO) is used to identify high inter-class variance features from the extracted image sets, which assists in selecting transformed images that can help improve hyperspectral classification performance. The selected hyperspectral images are fused via a Bacterial Foraging Optimization (BFO) model, which assists in reducing intra-class variance levels. The final set of selected images is intelligently augmented via Particle Swarm Optimization (PSO), which performs rotation, zooming, shifting, and brightness variation operations selectively. These augmented images are classified via a customized VGGNet-19-based Convolutional Neural Network (CNN) classifier that assists in continuously estimating accuracy levels for different application scenarios. Based on these accuracy levels, the model is reconfigured via hyperparameter tuning of GWO and PSO optimizers. Due to combining these models and incremental accuracy optimizations, the proposed model has improved its hyperspectral classification accuracy by 10.6% and precision by 10.4%, as compared to standard deep learning-based augmentation techniques.

INDEX TERMS Bacterial foraging optimization, grey wolf optimizer, hyperspectral images, particle swarm optimization, VGGNet-19.

The associate editor coordinating the review of this manuscript and approving it for publication was Mehul S. Raval.

I. INTRODUCTION

The hyperspectral images (HSIs) that are acquired via the use of remote sensing are made up of hundreds of continuous spectral bands that are very thin, and each pixel (vector) in the image offers a distinct description of the objects that are being investigated [46]. HSIs have a wide variety of applications, some of which include object identification, segmentation, and classification [47]. Support vector machines (SVMs), extreme learning machines (ELMs), and single-hidden layer feedforward networks are a few examples of machine learning approaches that have been used to extract information from high-dimensional hidden-state images (SHLFNs) [48]. Recent advancements in Earth observation missions have made it possible to capture HSI images of more excellent quality, including the addition of spectral bands and a higher resolution in space and spectral dimensions [49]. These improvements have been made possible due to recent advancements in imaging technology. Because of this, there has been a demand for an increase in both the storage capacity and the runtime via Adversarial Encoding Network (AEN) [4]. In this context, CNN models effortlessly combine spectral characteristics with spatial-contextual information from HSI data more effectively than prior DNN models; they have gained increasing traction as a powerful method for making sense of HSI data [5], [6]. As a result, deep learning methods based on CNNs have become the current gold standard for classifying HSI data [3]. Most of CNN's attempts to recognize HSI data include the problem of overfitting, which may be problematic. This difficulty adds to the challenge of learning already provided by the significant spectrum fluctuation characteristic of HSIs. According to various authors' understanding, the majority of the currently available strategies for reducing the impact of the overfitting problem [7] and enhancing CNN's capacity for generalization focus on amassing more training data during the phase of the process where it is being learned by including large geographical areas, sometimes with the help of geometric alterations [6]. Regularization methods are used in a variety of tactics. Techniques like dropout and Max Pooling were used in [5] work as a regularization. By giving an abstract representation of the convolved features, the max pooling layer aids in reducing both their spatial size and over-fitting. A regularization method called dropout is used to minimize over-fitting in neural networks. Deep learning models often employ dropout on the fully connected layers; however, it is also feasible to use dropout following the max-pooling layers, which augments image noise.

Recent attempts have also been made to improve the model architecture by increasing residual designs AEN [4] to offer each layer more data or expanding the connections between levels [8]. Both of these improvements were made very recently. There are just two examples included in this list. These strategies have been improved upon using a variety of methods, some of which include fully linked architectures [12], active learning [11], and pixel-pairs features (PPFs) [10]. These methods place a significant amount of emphasis on the performance of the output (Soft Max) layer to achieve their goals, contributing to the computation's complexity. The principal component analysis is a technique that is used by several scholars, including Chen et al. [12], to augment this level of analysis (PCA).

In comparison, the research in [11] enhances the model's generality by integrating data with greater levels of uncertainty. PPFs are used in the data pertinent to pixel neighborhoods in work presented in [10], which is an attempt very similar to those done to solve the problem of inconsistencies in the data. Data occlusion, also known as the inability of a remote sensor to view a portion of the Earth's surface due to factors such as the presence of an obstacle between the sensor and the two-dimensional target surface or adjacent three-dimensional objects, is a significant challenge that arises in the field of remote sensing. This may take place if, for instance, a three-dimensional object is positioned between the sensor and the two-dimensional surface that is being scanned. Since they cause a reduction in the amount of information in an image, blocking elements such as clouds, shadows, and others are to blame for this problem. The removal of data occlusions may be accomplished by many different strategies that have been established. These techniques were conceptualized after observing the human brain, which can operate most effectively in a three-dimensional environment [13], [14]. This concept may enhance the process of instructing machine learning strategies. From this brief review and the comprehensive review in the next section, it can also be observed that existing band-fusion-based augmentation models for hyperspectral images do not incorporate continuous efficiency enhancements and showcase higher complexity levels.

Moreover, the application of these models is limited to certain image types and thus cannot be scaled for broader use cases. To overcome these issues, section 3 of this text proposes designing a novel multimodal hybrid bioinspired model for the augmentation of hyperspectral imagery via iterative learning for continuous efficiency enhancements. The model was validated on multiple datasets, and its performance was compared for different datasets in section 4 of this text. Finally, this text is concluded with some context-specific observations about the proposed model and recommends various methods to further improve its performance levels.

The following is a summary of the study's key contributions:

- Proposed a novel bio-inspired augmentation methodology based on Fourier, Laplacian, Cosine, multimodal Wavelet, Mellin, and Z-Transform domains.
- PSO is used to optimize the geometric transformation parameters.
- It is possible to create a larger volume of images in less time that may be utilized as a remote sensing training data set for scene classification.
- The Python source code used in the experiments described in this article is made available to the public without charge (available at https://github.com/dipen0401/augmentation).

II. BRIEF REVIEW OF IMAGE AUGMENTATION MODELS

Data augmentation broadens the pool of information used to train a model. The key benefit is that the model becomes more stable and resistant to overfitting [57], [58]. The authors in [59] used flip, translation, and rotation in remote sensing scene classification. For instance, works in [15], [16], [17], and [18] propose the use of a Generative Adversarial Network (GAN), YOLOv5s, a multi-semantic global channel, and spatial joint attention module (MsGCS) for the estimation of augmented image sets for different application scenarios. These scenarios are extended in [19], [20], which discuss using Soft Augmentation-Based Siamese CNN (SAB SCNN) and different GANs for hyperspectral image sets. These models are highly scalable but showcase higher complexity, which limits their speed performance levels. To overcome this issue, works in [21], [22], [23], [24], and [25] propose using Hapke equations, Local Bias CNN, Hierarchical Amortized GAN, Cycle GAN, and Attention Networks for the estimation of augmented image sets. These sets are obtained via simplified augmentation operations and can be applied to multimodal application scenarios. Similarly, work in [26], [27], [28], [29], and [30] proposes the use of a Convolutional Network with Twofold Feature Augmentations, Proto-MaxUp (PM), Conditional GAN, Hierarchical CNN with Soft Augmentation (HCNN SA), and Mask Region CNN, for estimation of high-density image sets under different application scenarios. These models can improve classification efficiency under multimodal scenarios.

Models that propose the use of Low-Pass Activation Function with DCT Augmentation [31], Spatial Feature Enhanced Unets [32], Localization-Aware Adaptive Pairwise Margin Loss [33], Bitplane Information Recombination [34], improved YoLo [35], auto-updating multitemporal matrix factorization with spatio-spectral channel augmentation (AMMF SSCA) [36], Spectral Index Generative Adversarial Network (SIGAN) [37], and pixel-level augmentations [38], that assist in improving classification performance for various application sets. These models aim to optimize the augmentations via pre-emptive analysis, enabling high accuracy and low complexity classification operations. Models discussed in [39], [40], [41], and [42] further extend these methods via integrating multimodal GAN, small target GAN, Siamese CNN, and Global Spatial with Local Spectral Similarity levels for satellite image sets. These models showcase higher complexity but enable high-accuracy augmentations for larger image sets. Similar models are proposed in [43], [44], and [45] that use deformable convolutional networks (DCNs), Generative Motion Models, and fully convolutional neural networks (FCN) for simplified classification with moderate accuracy levels. But these models do not incorporate continuous efficiency enhancements and showcase higher complexity levels.

Moreover, the application of these models is limited to certain image types and thus cannot be scaled for broader use cases. To overcome these issues, the next section of this text proposes a design of a novel multimodal hybrid bioinspired model for the augmentation of hyperspectral imagery via iterative learning for continuous efficiency enhancements. The proposed model was validated under different application sets, and their performance was evaluated under large-scale scenarios.

III. DESIGN OF THE PROPOSED MODEL

Based on the review of existing hyperspectral image augmentation models, these models use high-complexity feature analysis to improve classification performance under different use cases. When combined with intelligent band-fusion methods, such models allow the augmentation model to enhance its classification efficiency under other use cases. Existing band-fusion-based augmentation models for hyperspectral images do not incorporate continuous efficiency enhancements and showcase higher complexity levels. Moreover, the application of these models is limited to certain image types and thus cannot be scaled for broader use cases. To overcome these issues, this section discusses the design of a novel multimodal hybrid bioinspired model for augmentation hyperspectral imagery via iterative learning for continuous efficiency enhancements. The flow of the model is depicted in Fig. 1. It can be observed that the proposed model initially represents input images into Fourier, Laplacian, Cosine, multimodal Wavelet, Mellin, and Z-Transform domains, which will assist in representing the images in multimodal domains. These transformed image sets are passed through a convolutional filter to extract windowed feature sets. A Grey Wolf Optimizer (GWO) [62] is used to identify high inter-class variance features from the extracted image sets, which assists in selecting transformed images that can improve hyperspectral classification performance. The selected hyperspectral images are fused via a Bacterial Foraging Optimization (BFO) model [50], which assists in reducing intra-class variance levels. The final set of selected images is intelligently augmented via Particle Swarm Optimization (PSO) [51], which performs rotation, zooming, shifting, and brightness variation operations selectively. These augmented images are classified via a customized VGGNet-19-based Convolutional Neural Network (CNN) classifier [59], [61] that assists in continuously estimating accuracy levels for different application scenarios.

Thus, all the collected satellite images are initially passed through a transformation process. This process uses the following transforms,

- Fourier transformation is evaluated via (1) and used to represent input pixels as frequency components, thus assisting in identifying any frequent patterns in the image sets. [53]

$$\mathrm{F}(\mathrm{r}, \mathrm{c}, \mathrm{b}) = \frac{1}{\mathrm{R} * \mathrm{C} * \mathrm{B}} \sum_{\mathrm{i}=1}^{\mathrm{R}} \sum_{\mathrm{j}=1}^{\mathrm{C}} \sum_{\mathrm{l}=1}^{\mathrm{B}} \mathrm{I}(\mathrm{r}, \mathrm{c}, \mathrm{b}) * \exp\left(\frac{2 * \sqrt{-1} * \Pi * \mathrm{i} * \mathrm{j} * \mathrm{l}}{\mathrm{R} * \mathrm{C} * \mathrm{B}}\right) \tag{1}$$

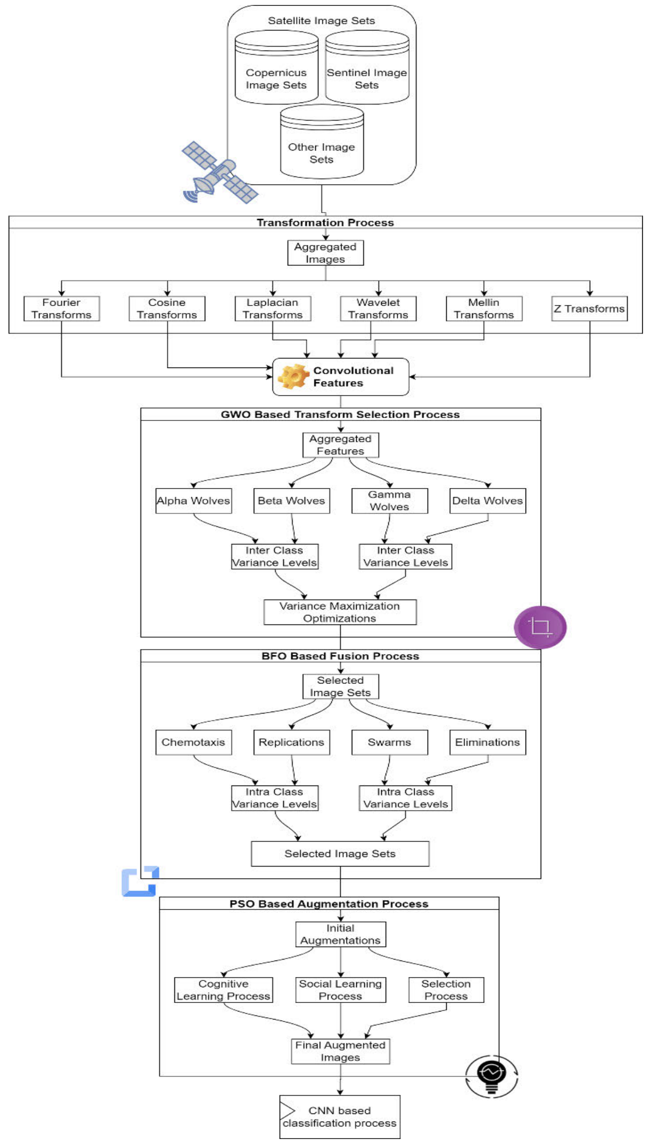

FIGURE 1. **The flow of the proposed augmentation process.**

- Laplacian transformation is evaluated via equation 2 and used to represent input pixels as equational entities, thus assisting in evaluating temporal feature sets [56].

$$L(r,c,b) = \frac{b}{\Pi}\sum_{i=1}^{R}\sum_{j=1}^{C}\frac{I(r,c,b)}{(r-i)^2+(c-j)^2+(b)^2} \tag{2}$$

- Cosine transformation is evaluated via (3) and used to represent input pixels as entropy levels, thus assisting in identifying maximal energy patterns in the image sets [55].

$$DCT(r,c,b) = \frac{1}{2\sqrt{RCB}}\sum\nolimits_{i=1}^{R}\sum\nolimits_{j=1}^{C}\sum\nolimits_{l=1}^{B} I(r,c,b) * \cos\left(\frac{(2i+1)\Pi\sqrt{-1}}{2R}\right) * cos\left(\frac{(2j+1)\Pi\sqrt{-1}}{2C}\right) * \cos\left(\frac{(2l+1)\Pi\sqrt{-1}}{2B}\right) \tag{3}$$

- Multimodal Wavelet transformation is evaluated via (4), (5), (6), & (7) and used to represent input pixels as approximate, diagonal, vertical, and detail components, thus assisting in the identification of directional patterns in the image sets [54].

$$Wa(r,c,b) = \frac{I(r,c,b)+I(r,c+1,b)+I(r+1,c,b)+I(r+1,c+1,b)}{4} \tag{4}$$

$$Wh(r,c,b) = \frac{I(r,c,b)-I(r,c+1,b)+I(r+1,c,b)+I(r+1,c+1,b)}{4} \tag{5}$$

$$Wv(r,c,b) = \frac{I(r,c,b)+I(r,c+1,b)-I(r+1,c,b)+I(r+1,c+1,b)}{4} \tag{6}$$

$$Wd(r,c,b) = \frac{I(r,c,b)-I(r,c+1,b)+I(r+1,c,b)-I(r+1,c+1,b)}{4} \tag{7}$$

where, Wa, Wh, Wv, & Wd represent approximate, horizontal, vertical, and diagonal wavelet components respectively.

- Mellin transformation is evaluated via (8) and used to represent input pixels as variance-independent sets, thus assisting in identifying variance levels in the image sets.

$$M(r,c,b) = \frac{1}{2\Pi\sqrt{-1}*R*C*B}\sum\nolimits_{i=1}^{R}\sum\nolimits_{j=1}^{C} \times \sum\nolimits_{l=1}^{B} I(r,c,b)^{-(ijl)} \tag{8}$$

- Z-Transform transformation is evaluated via (9) and used to represent input pixels as frequency components and assists in the identification of stability levels of pixel sets [53].

$$Z(r,c,b) = \frac{\sum_{i=1}^{R}\sum_{j=1}^{C}\sum_{l=1}^{B} I(r,c,b) * z^{-rcb}}{RCB} \tag{9}$$

Based on these transforms, each band of the input image is represented in multiple domains. These domain sets are represented into convolutional feature sets via (10),

$$Conv_{out_{i,j}}(band) = \sum\nolimits_{a=-\frac{m}{2}}^{\frac{m}{2}}\sum\nolimits_{b=-\frac{n}{2}}^{\frac{n}{2}} I \times (i-a, j-b, band) * ReLU\left(\frac{m}{2}+a, \frac{n}{2}+b\right) \tag{10}$$

where m, n represents window sizes, a, b represents stride sizes, and ReLU represents a rectilinear unit which is used to activate the feature sets via (11),

$$\begin{aligned} ReLU\,(x, y) &= Max\,(x, y) \\ &\quad when\; x > 0 \quad \&\, y > 0,\; \textbf{\textit{else}}\; x \\ &\quad when\; x > 0, \quad \textbf{\textit{else}}\; y \\ &\quad when\; y > 0, \quad \textbf{\textit{else}}\; 0\, for\; other\; cases \end{aligned} \tag{11}$$

These feature sets are processed via a Grey Wolf Optimizer [62] that works via the following process,

- To initialize the GWO-based feature selection process, setup the following constants,
  - Total GWO iterations = N_i
  - Total GWO Wolves = N_w
  - Rate of cognitive learning between Wolves = L_w

  To set up initial Wolf configurations, generate N_w Wolves as per the following process,
  Stochastically select N features via (12),

$$N = STOCH\left(L_w * N_f, N_f\right) \tag{12}$$

  STOCH represents a stochastic Markovian process used to generate number sets, while Nf represents some extracted feature sets.
  For the selected feature sets, identify their inter-class variance levels for each class via (13),

$$icv\,(m) = \sqrt{\frac{\sum_{a=1}^{m} \left(x_a - \frac{\sum_{i=1}^{m} \sqrt{\frac{\sum_{j=1}^{n} \left(x_j - \frac{\sum_{k=1}^{n} x_k}{n}\right)^2}{n-1}}}{m}\right)^2}{m-1}} \tag{13}$$

  where m represents total features in the current class, icv represents their interclass variance levels, x represents the extracted features, and n represents features in other classes.
  - This variance is estimated for all classes, and then Wolf fitness is calculated via (14),

$$f = \frac{1}{c} \sum_{i=1}^{c} icv\,(m)_i \tag{14}$$

    where c represents the total number of classes present in the image sets.
  - This fitness is estimated for all Wolves, and then a Wolf fitness threshold is calculated via (15),

$$f_{th} = \frac{1}{N_w} \sum_{i=1}^{N_w} f_i * L_w \tag{15}$$

- Based on this evaluation, Wolves are reconfigured as per the following conditions,
  - Mark the current Wolf as 'Alpha,' if f > 2 * f_{th}
  - Else, mark the current Wolf as 'Beta,' if f > f_{th}
  - Else, mark the current Wolf as 'Gamma,' if f > $f_{th} * L_r$
  - Else, mark the Wolf as 'Delta' and use it for optimization processes
- Regenerate all Wolves that are marked as 'Delta' as per (12), (13), and (14)
- Reconfigure all 'Gamma' & 'Beta' Wolves by replacing their features from 'Beta' & 'Alpha' Wolves respectively, where variance levels are higher, as per (16)

$$f\,(New) = f\,(Old)\,|_{f > f_{th}} \tag{16}$$

  where *f(New)* represents new features for 'Gamma' and 'Beta' Wolves, while $f\,(Old)$ represents highly variant features from respective 'Beta' and 'Alpha' Wolf configurations [62].
- This process is repeated for N_i iterations.
  At the end of the final iteration, select unique features from all 'Alpha' Wolves, and use their respective transform images for further augmentation. The chosen transform images from different bands are fused via a BFO-based optimization model that works as per the following process [50],
- To initialize the fusion optimization process, setup the following constants,
  - Total number of bacteria in the swarms (NB)
  - Total iterations used for optimization (NI)
  - Elimination constant (C_e)
  - Regeneration constant (C_r)
- Loop through NI iterations and perform the following process,
  - Generate NB bacteria chemotaxis as per the following process,
    - Select N transformed images for fusion as per (17),

$$\mathrm{N} = \mathrm{STOCH}\,(\mathrm{C_r} * \mathrm{NI}, \mathrm{NI}) \tag{17}$$

      where *NI* represents the total number of highly variant images identified from the GWO process.
    - Fuse these images as per Brovey fusion via (18),

$$F_{out} = \frac{F_{in}}{\sum_{i=1}^{B} I_i} * P \tag{18}$$

      where, F_{in} & P represents input multispectral & panchromatic image bands, while B represents total bands in the multispectral images.
    - For each of these images, convolutional features are extracted via (10), and then their intra-class variance is estimated via (19),

$$iccv\,(m) = \sqrt{\frac{\sum_{i=1}^{m} \sqrt{\frac{\sum_{j=1}^{n} \left(x_j - \frac{\sum_{k=1}^{m} x_k}{m}\right)^2}{m-1}}}{m}} \tag{19}$$

      where m represents total images in the current class, iccv represents their intra-class variance levels.

- Based on these values, bacteria fitness is estimated via (20),

$$f_b = \left(C_e + \frac{1}{C_r}\right) * \sum_{i=1}^{c} \frac{iccv\,(m)_i}{c} \tag{20}$$

- This fitness is estimated for each bacterium, and then their configuration is updated via (21),

$$\begin{aligned} f\,(New) &= \sum\nolimits_{i=1}^{NB} -f_b * \exp\left(-C_e\right) * \left(C_e + \frac{1}{C_r}\right) \\ &\quad + \sum\nolimits_{i=1}^{NB} -iccv\,(m)_i \\ &\quad * \exp\left(-C_e\right) * \left(C_e + \frac{1}{C_r}\right) \end{aligned} \tag{21}$$

- A Bacterium with $f_b > f\,(New)$ *is* passed to the next iteration, while others are reconfigured as per the BFO process [50],

- After repeating this process for NI iterations, select bacteria configurations with maximum fitness levels.
The selected bacterium represents fused images that can be used for efficient augmentation operations. These operations are controlled via a Particle Swarm Optimization (PSO) Model that selectively performs different augmentations. This PSO Model works via the following process [51],
- Initially set up following PSO constants for efficient augmentations,
    - Total optimization iterations (N_i)
    - Total optimization particles (N_p)
    - The cognitive learning rate for these particles (L_c)
    - The social learning rate for these particles (L_s)
- To start the PSO optimization process, generate N_p particles as follows,
    - Select N augmentation operations as per (22),

$$N = STOCH\,(L_c * NA, NA\,) \tag{22}$$

where NA represents the total number of operations available to perform augmentations, and NA ∈ (Shift, Scale, Rotate, Zoom, Brightness) [52]

- Based on this value of N, perform the augmentation and estimate the accuracy of augmentation via the CNN-based classification model [59], which is depicted in Fig. 2 as follows:
- The CNN model [59] extracts convolutional features from the input images and then uses a series of Max Pooling and Dropout operations.
- These operations use a Max Pooling threshold which is estimated as per (23),

$$f_{th} = \left(\frac{1}{X_k} * \sum_{x \in X_k} x^{p_k}\right)^{1/p_k} \tag{23}$$

where X represents the extracted convolutional features and p represents dropout probability levels.

TABLE 1. Parameters used in the training model.

Sr. No	Parameters	Value
1	Total layers	16
2	Window size	8, 16, 32, 64, 128, 256
3	Kernel size	3, 5, 7, 9, 11, 13, 15
4	Activation function	Softmax

- The selected features are classified via a fully connected neural network (FCNN) based classification layer that uses Soft Max activations as per (24),

$$c_{out} = SoftMax\left(\sum_{i=1}^{N_f} f_i * w_i + b\right) \tag{24}$$

where w & b represent weights and biases of the convolutional layers.

- Based on these operations, particle fitness levels are estimated as per (25),

$$f_p = \sum_{i=1}^{N} \frac{C_i}{T_i} \tag{25}$$

where C & T represent correctly classified and total images used for the classification process, respectively.

- This fitness is estimated for all particles.
- Current fitness is marked as 'Particle Best,' while the highest fitness is marked as 'Global Best' levels.
- Now, loop through N_i iterations, and perform the following tasks,
    - Update the number of augmentation operations in each particle [51] via (26),

$$\begin{aligned} A\,(New) &= A\,(Old) + L_c * s_1 * |A\,(Old) - PBest| \\ &\quad + L_s * s_2 * |A\,(Old) - GBest| \end{aligned} \tag{26}$$

where, A (Old) & A(New) represents old and new augmentation operations, while s_1 & s_2 represents two stochastic number sets.

- At the end of the final iteration, identify the particle with the highest fitness levels and use its augmentation operations to optimize classification performance for satellite image sets.
Based on these optimization processes, the model can identify efficient augmentation operations that can effectively classify different satellite images. This performance is estimated in terms of classification accuracy, precision, recall, and computational delay in the next section of this manuscript.
The parameters used in the training models have been listed in Table 1.

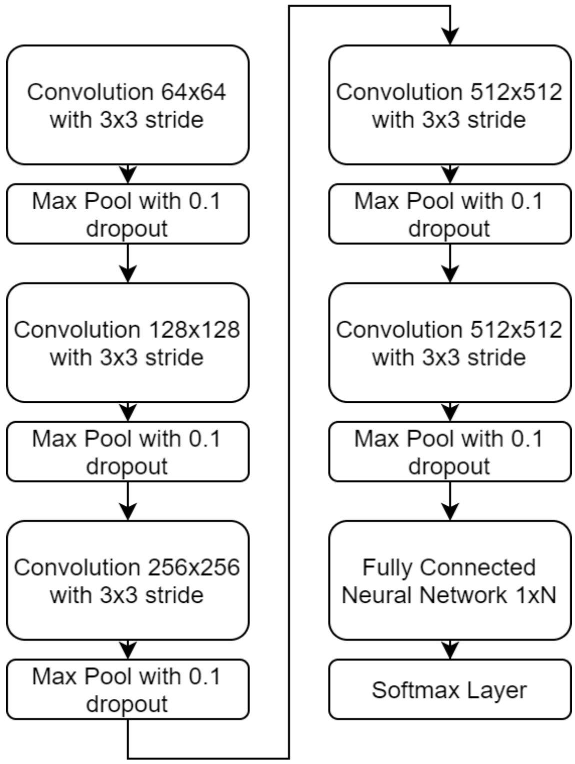

FIGURE 2. Design of the CNN model for classification operations.

IV. THE RESULT ANALYSIS & COMPARISON WITH STANDARD AUGMENTATION TECHNIQUES

The proposed model initially uses a multimodal image representation framework capable of extracting Wavelet components, Fourier Components, Cosine Components, Laplacian Components, Mellin Transformations, and Z Transformations. These image sets are processed via a GWO-based image selection framework that uses convolutional feature sets for efficient inter-class image representations. These selected image sets are further optimized via a BFO-based intra-class feature variance optimization process. Due to the use of GWO and BFO, the image-chosen are observed to have higher variance levels, which assists in optimizing classification performance. These selected images are augmented via a PSO-based optimization process, which helps choose efficient augmentation operations validated by a CNN-based classifier to maximize accuracy levels. To evaluate the performance of this model, it was validated on the following datasets,

Sentinel image sets obtained from Google Earth Engine

- Copernicus image sets obtained from Kaggle
- IEEE data port sets for different areas

These sets were aggregated to form 300k images, of which 70% were used to train the model, while 15% each was used for validation & testing purposes. Based on this evaluation, the accuracy of the classification [60] (A_c) was estimated via (27),

$$A_c = \frac{S_c}{S_T} \tag{27}$$

where S_C & S_T are the total number of correctly classified satellite image sets and used image sets, respectively. Results of these augmentations can be observed in Fig. 3(a), Fig. 3(b), and Fig. 3(c), wherein different satellite images were used for the scene classification process.

TABLE 2. Classification accuracy for different satellite image sets.

VTI	Ac AEN [4]	Ac SAB SCNN [19]	Ac SI GAN [37]	Ac MBA HIL
1k	88.10	88.34	85.81	95.00
2k	88.25	88.68	86.05	95.26
3k	88.40	89.00	86.29	95.53
5k	88.55	89.34	86.53	95.79
10k	88.71	89.68	86.76	96.05
25k	88.86	90.00	87.00	96.31
50k	88.99	90.34	87.24	96.57
75k	89.14	90.68	87.47	96.83
100k	89.29	91.02	87.71	97.09
125k	89.44	91.35	87.95	97.35
150k	89.60	91.68	88.19	97.61
200k	89.74	92.02	88.43	97.88
250k	89.90	92.35	88.66	98.14
300k	90.04	92.69	88.91	98.40

Based on similar image sets, these accuracy levels were estimated for all validation & test images (VTI) and were compared with AEN [4], SAB SCNN [19], and SI GAN [37] in Table 2 as follows:

As per this analysis and Fig. 4, it can be observed that the proposed model is capable of improving the accuracy of classification by 9.2% when compared with AEN [4], 6.1% when compared with SAB SCNN [19], and 10.6% when compared with SI GAN [37] under different image sets. This is possible due to the incorporation of accuracy during the selection of PSO-based augmentation operations. Due to this, the model can showcase superior accuracy performance under large image sets. Similarly, the precision of classification [60] was evaluated via (28),

$$P_c = \frac{S_{CI}}{S_T} \tag{28}$$

where S_{CI} and S_T represents the total number of correctly identified images in the incorrect category and the total number of images used for the classification process. This precision can be observed in Table 3 as follows:

As per this analysis and Fig. 5, it can be observed that the proposed model is capable of improving the precision of classification by 10.4% when compared with AEN [4], 3.9% when compared with SAB SCNN [19], and 7.3% when compared with SI GAN [37] under different image sets.

This is possible due to the incorporation of inter-class variance levels during the selection of fusion operations and

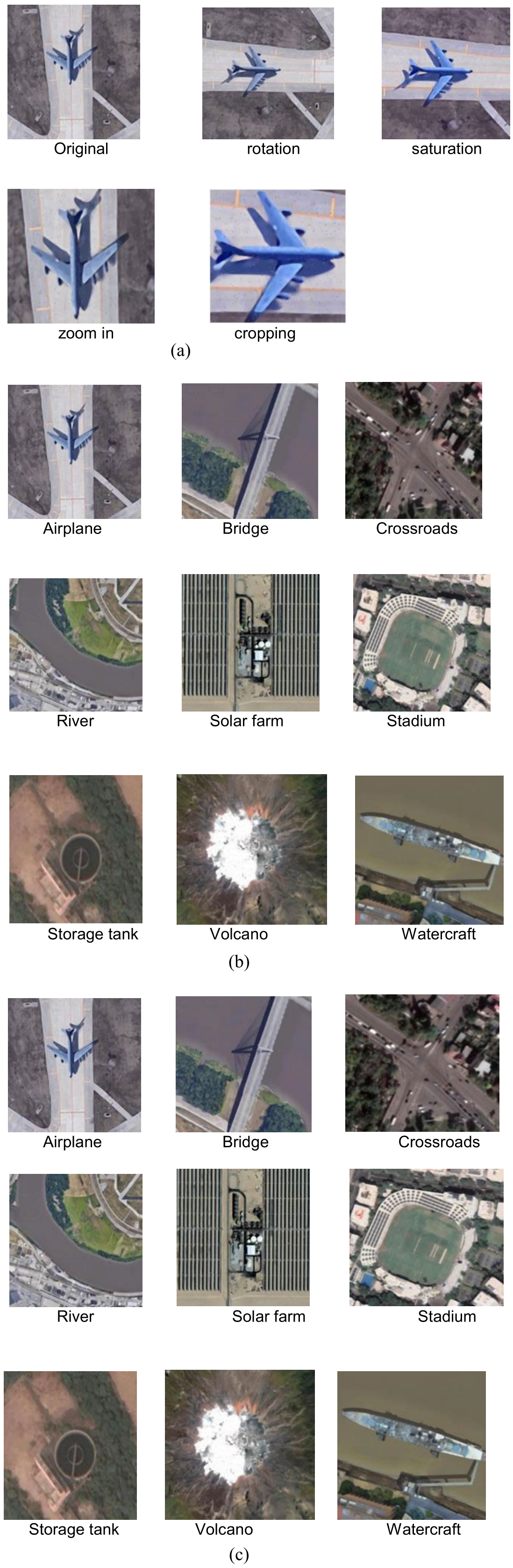

FIGURE 3. (a) Use of basic transformation techniques for augmentation. (b) Some scene classifications of the augmented image sets. (c) Use of the augmentation for different application sets.

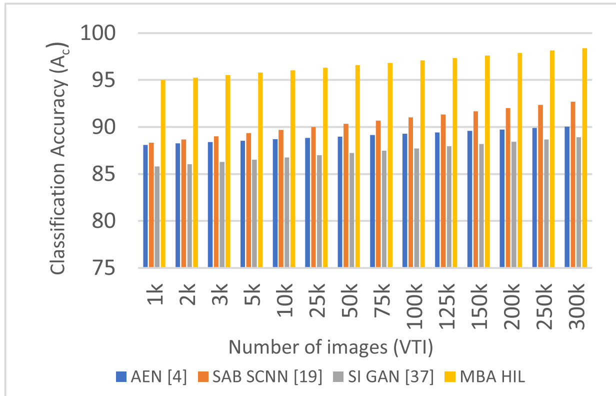

FIGURE 4. Classification accuracy for different satellite image sets.

TABLE 3. Classification precision for different satellite image sets.

VTI	Pc AEN [4]	Pc SAB SCNN [19]	Pc SI GAN [37]	Pc MBA HIL
1k	83.68	86.58	84.98	91.24
2k	83.83	86.90	85.21	91.48
3k	83.98	87.22	85.45	91.74
5k	84.13	87.54	85.69	91.98
10k	84.27	87.86	85.91	92.22
25k	84.40	88.19	86.14	92.47
50k	84.54	88.53	86.36	92.71
75k	84.67	88.86	86.60	92.97
100k	84.82	89.19	86.83	93.21
125k	84.96	89.51	87.05	93.46
150k	85.11	89.84	87.29	93.71
200k	85.26	90.17	87.52	93.96
250k	85.40	90.49	87.76	94.21
300k	85.55	90.82	87.99	94.45

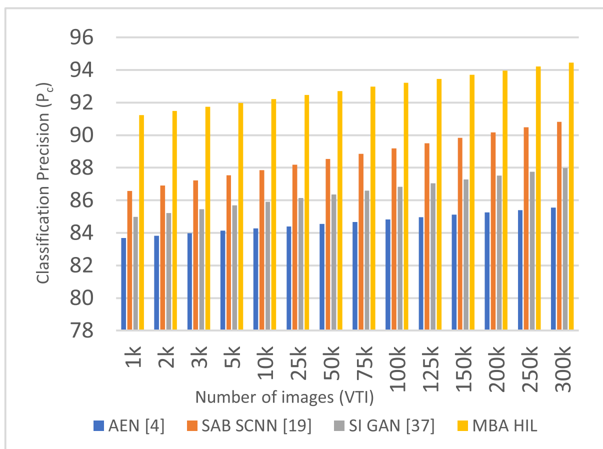

FIGURE 5. Classification precision for different satellite image sets.

the use of accuracy during the selection of PSO-based augmentation operations. Due to these integrations, the model can showcase superior precision performance under large image sets. Similarly, the recall [60] was evaluated via (29),

$$R_c = \frac{S_{CC}}{S_T} \tag{29}$$

TABLE 4. Classification recall for different satellite image sets.

VTI	Rc AEN [4]	Rc SAB SCNN [19]	Rc SI GAN [37]	Rc MBA HIL
1k	68.71	79.47	71.17	88.67
2k	68.84	79.78	71.38	88.93
3k	68.97	80.08	71.57	89.19
5k	69.09	80.39	71.76	89.43
10k	69.21	80.69	71.95	89.67
25k	69.33	81.00	72.14	89.91
50k	69.43	81.31	72.33	90.16
75k	69.53	81.61	72.52	90.40
100k	69.65	81.92	72.72	90.64
125k	69.76	82.22	72.93	90.89
150k	69.88	82.53	73.13	91.13
200k	70.01	82.83	73.32	91.38
250k	70.13	83.14	73.52	91.63
300k	70.26	83.44	73.71	91.87

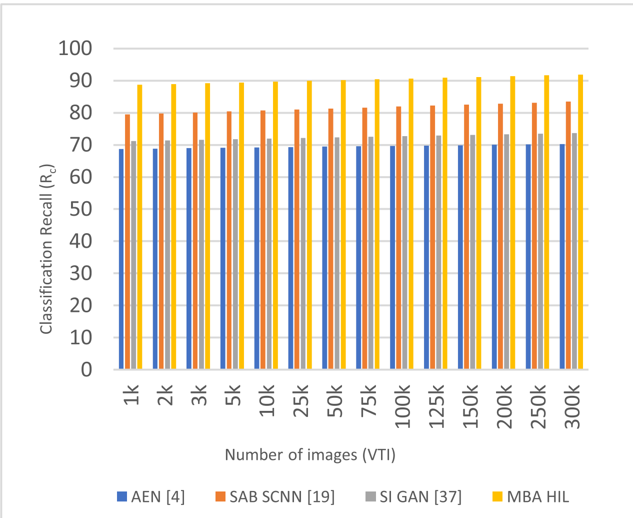

FIGURE 6. Classification recall for different satellite image sets.

where S_{CC} represents the total number of satellite images correctly identified into correct categories. The recall levels can be observed in Table 4 as follows:

As per this analysis and Fig. 6, it can be observed that the proposed model is capable of improving recall of classification by 30.7% when compared with AEN [4], 10.1% when compared with SAB SCNN [19], and 24.6% when compared with SI GAN [37] under different image sets. This is possible due to the use of intra-class & inter-class variance levels during the identification of multimodal sets and the selection of fusion operations, with the help of accuracy during the selection of PSO-based augmentation operations. Due to these integrations, the model can showcase superior recall performance under large image sets. Similarly, the classification delay can be observed from Table 5 as follows:

As per this analysis and Fig. 7, it can be observed that the proposed model is capable of decreasing the classification delay by 32.7% when compared with AEN [4], 28.5% when compared with SAB SCNN [19], and 17.04% when compared with SI GAN [37] under different image sets.

TABLE 5. Classification delay for different satellite image sets.

VTI	Dc AEN [4]	Dc SAB SCNN [19]	Dc SI GAN [37]	Dc MBA HIL
1k	56.11	51.49	44.92	37.25
2k	56.21	51.69	45.05	37.36
3k	56.31	51.88	45.18	37.46
5k	56.41	52.07	45.30	37.56
10k	56.51	52.26	45.42	37.66
25k	56.61	52.45	45.54	37.76
50k	56.70	52.64	45.66	37.87
75k	56.79	52.83	45.78	37.97
100k	56.89	53.03	45.90	38.07
125k	56.99	53.23	46.02	38.18
150k	57.08	53.42	46.15	38.28
200k	57.18	53.62	46.27	38.38
250k	57.28	53.81	46.39	38.48
300k	57.38	54.01	46.52	38.59

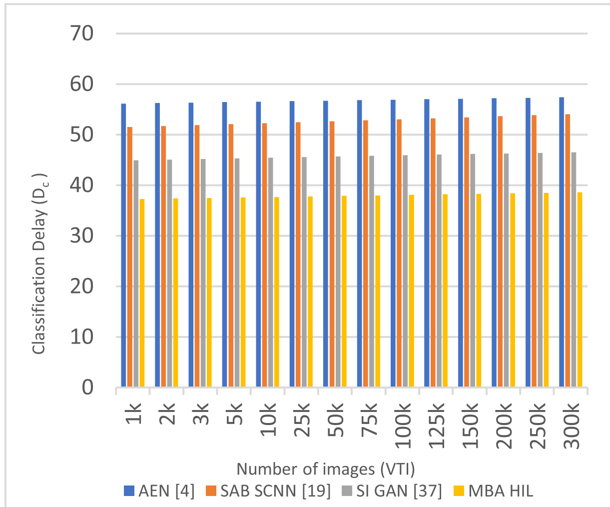

FIGURE 7. Classification delay for different satellite image sets.

This is possible due to the identify optimum image sets for classification under various satellite image types. Due to these integrations, the model can showcase high-speed performance under large image sets. This makes the model highly useful for a wide variety of classification scenarios.

V. CONCLUSION

Our research has observed that data augmentation is a significant way to keep a model from becoming too good at what it does and to lower the cost of labeling and cleaning the raw dataset. This study proposed a new bio-inspired model for improving the augmentation of hyperspectral imagery that uses the domains of Fourier, Laplacian, Cosine, multimodal Wavelet, Mellin, and Z-Transform. In our findings, we observed that Particle Swarm Optimization helps to find the best values for the parameters of geometric transformations, such as rotation, shifting, etc. When we compared our proposed model with existing models like AEN, SAB SCNN, and SI GAN, we learned that it improved the classification accuracy by 9.2%, 6.1%, and 10.6%, respectively. With the incorporation of inter-class variance levels during the selection of fusion operations and the use of accuracy during the selection of PSO-based augmentation operations, we noticed that the proposed model has improved classification precision by 10.4%, 3.9%, and 7.3% as compared to AEN, SAB SCNN, and SI GAN, respectively, for different image sets. Furthermore, we observed that the proposed model could improve recall of classification by 30.75% compared with AEN, 10.1% with SAB SCNN, and 24.6% with SI GAN due to the use of intra-class & inter-class variance levels during the identification of multimodal sets, and selection of fusion operations, with use of accuracy during the selection of PSO based augmentation operations.

The model can be further improved by combining low-complexity and high-density feature extraction techniques as a future enhancement. We can improve classification performance using hybrid bioinspired models, autoencoders, gated recurrent units (GRUs), or other deep-learning methods.

AUTHOR CONTRIBUTIONS

All authors have contributed equally to this work.

CONFLICTS OF INTEREST

The authors declare no conflict of interest.

REFERENCES

[1] H.-S. Ham, H.-S. Lee, J.-W. Chae, H. C. Cho, and H.-C. Cho, "Improvement of gastroscopy classification performance through image augmentation using a gradient-weighted class activation map," *IEEE Access*, vol. 10, pp. 99361–99369, 2022, doi: 10.1109/ACCESS.2022.3207839.

[2] R. Zhang, W. Lu, X. Wei, J. Zhu, H. Jiang, Z. Liu, J. Gao, X. Li, J. Yu, M. Yu, and R. Yu, "A progressive generative adversarial method for structurally inadequate medical image data augmentation," *IEEE J. Biomed. Health Informat.*, vol. 26, no. 1, pp. 7–16, Jan. 2022, doi: 10.1109/JBHI.2021.3101551.

[3] Z. Li, C. Zheng, H. Shu, and S. Wu, "Dual-scale single image dehazing via neural augmentation," *IEEE Trans. Image Process.*, vol. 31, pp. 6213–6223, 2022, doi: 10.1109/TIP.2022.3207571.

[4] S. Du, J. Hong, Y. Wang, K. Xing, and T. Qiu, "Physical-related feature extraction from simulated SAR image based on the adversarial encoding network for data augmentation," *IEEE Geosci. Remote Sens. Lett.*, vol. 19, pp. 1–5, 2022, doi: 10.1109/LGRS.2021.3100642.

[5] X. Xu, T. Sanford, B. Turkbey, S. Xu, B. J. Wood, and P. Yan, "Shadow-consistent semi-supervised learning for prostate ultrasound segmentation," *IEEE Trans. Med. Imag.*, vol. 41, no. 6, pp. 1331–1345, Jun. 2022, doi: 10.1109/TMI.2021.3139999.

[6] R. Yamashita, J. Long, S. Banda, J. Shen, and D. L. Rubin, "Learning domain-agnostic visual representation for computational pathology using medically-irrelevant style transfer augmentation," *IEEE Trans. Med. Imag.*, vol. 40, no. 12, pp. 3945–3954, Dec. 2021, doi: 10.1109/TMI.2021.3101985.

[7] X. Shang, S. Han, and M. Song, "Iterative spatial-spectral training sample augmentation for effective hyperspectral image classification," *IEEE Geosci. Remote Sens. Lett.*, vol. 19, pp. 1–5, 2022, doi: 10.1109/LGRS.2021.3131373.

[8] H. Chen, W. Li, and Z. Shi, "Adversarial instance augmentation for building change detection in remote sensing images," *IEEE Trans. Geosci. Remote Sens.*, vol. 60, 2022, Art. no. 5603216, doi: 10.1109/TGRS.2021.3066802.

[9] J. Liu, Z. Wang, Y. Zhang, A. Traverso, A. Dekker, Z. Zhang, and Q. Chen, "CycleGAN clinical image augmentation based on mask self-attention mechanism," *IEEE Access*, vol. 10, pp. 105942–105953, 2022, doi: 10.1109/ACCESS.2022.3211670.

[10] C. You, Y. Zhou, R. Zhao, L. Staib, and J. S. Duncan, "SimCVD: Simple contrastive voxel-wise representation distillation for semi-supervised medical image segmentation," *IEEE Trans. Med. Imag.*, vol. 41, no. 9, pp. 2228–2237, Sep. 2022, doi: 10.1109/TMI.2022.3161829.

[11] S. Nesteruk, S. Illarionova, T. Akhtyamov, D. Shadrin, A. Somov, M. Pukalchik, and I. Oseledets, "XtremeAugment: Getting more from your data through combination of image collection and image augmentation," *IEEE Access*, vol. 10, pp. 24010–24028, 2022, doi: 10.1109/ACCESS.2022.3154709.

[12] C. Chen, Y. Xing, H. Gao, L. Zhang, and Z. Chen, "Sam's net: A self-augmented multistage deep-learning network for end-to-end reconstruction of limited angle CT," *IEEE Trans. Med. Imag.*, vol. 41, no. 10, pp. 2912–2924, Oct. 2022, doi: 10.1109/TMI.2022.3175529.

[13] Q. Xiao, B. Liu, Z. Li, W. Ni, Z. Yang, and L. Li, "Progressive data augmentation method for remote sensing ship image classification based on imaging simulation system and neural style transfer," *IEEE J. Sel. Topics Appl. Earth Observ. Remote Sens.*, vol. 14, pp. 9176–9186, 2021, doi: 10.1109/JSTARS.2021.3109600.

[14] L. S. Hesse, G. Kuling, M. Veta, and A. L. Martel, "Intensity augmentation to improve generalizability of breast segmentation across different MRI scan protocols," *IEEE Trans. Biomed. Eng.*, vol. 68, no. 3, pp. 759–770, Mar. 2021, doi: 10.1109/TBME.2020.3016602.

[15] C. Tiago, A. Gilbert, A. S. Beela, S. A. Aase, S. R. Snare, J. Sprem, and K. McLeod, "A data augmentation pipeline to generate synthetic labeled datasets of 3D echocardiography images using a GAN," *IEEE Access*, vol. 10, pp. 98803–98815, 2022, doi: 10.1109/ACCESS.2022.3207177.

[16] C. Huang, J. Zhao, Y. Yu, and H. Zhang, "Comprehensive sample augmentation by fully considering SSS imaging mechanism and environment for shipwreck detection under zero real samples," *IEEE Trans. Geosci. Remote Sens.*, vol. 60, pp. 1–14, 2022, doi: 10.1109/TGRS.2021.3116671.

[17] M. Wang, W. Zhu, F. Shi, J. Su, H. Chen, K. Yu, Y. Zhou, Y. Peng, Z. Chen, and X. Chen, "MsTGANet: Automatic drusen segmentation from retinal OCT images," *IEEE Trans. Med. Imag.*, vol. 41, no. 2, pp. 394–406, Feb. 2022, doi: 10.1109/TMI.2021.3112716.

[18] W. Wang, Y. Chen, X. He, and Z. Li, "Soft augmentation-based Siamese CNN for hyperspectral image classification with limited training samples," *IEEE Geosci. Remote Sens. Lett.*, vol. 19, pp. 1–5, 2022, doi: 10.1109/LGRS.2021.3103180.

[19] A. Anaam, H. M. Bu-Omer, and A. Gofuku, "Studying the applicability of generative adversarial networks on HEp-2 cell image augmentation," *IEEE Access*, vol. 9, pp. 98048–98059, 2021, doi: 10.1109/ACCESS.2021.3095391.

[20] K. Qin, F. Ge, Y. Zhao, L. Zhu, M. Li, C. Shi, D. Li, and X. Zhou, "Hapke data augmentation for deep learning-based hyperspectral data analysis with limited samples," *IEEE Geosci. Remote Sens. Lett.*, vol. 18, no. 5, pp. 886–890, May 2021, doi: 10.1109/LGRS.2020.2989796.

[21] Y. Kim, A. F. M. S. Uddin, and S.-H. Bae, "Local augment: Utilizing local bias property of convolutional neural networks for data augmentation," *IEEE Access*, vol. 9, pp. 15191–15199, 2021, doi: 10.1109/ACCESS.2021.3050758.

[22] L. Sun, J. Chen, Y. Xu, M. Gong, K. Yu, and K. Batmanghelich, "Hierarchical amortized GAN for 3D high resolution medical image synthesis," *IEEE J. Biomed. Health Informat.*, vol. 26, no. 8, pp. 3966–3975, Aug. 2022, doi: 10.1109/JBHI.2022.3172976.

[23] Q. H. Cap, H. Uga, S. Kagiwada, and H. Iyatomi, "LeafGAN: An effective data augmentation method for practical plant disease diagnosis," *IEEE Trans. Autom. Sci. Eng.*, vol. 19, no. 2, pp. 1258–1267, Apr. 2022, doi: 10.1109/TASE.2020.3041499.

[24] C.-H. Lin, C.-S. Lin, P.-Y. Chou, and C.-C. Hsu, "An efficient data augmentation network for out-of-distribution image detection," *IEEE Access*, vol. 9, pp. 35313–35323, 2021, doi: 10.1109/ACCESS.2021.3062187.

[25] C.-H. Hua, K. Kim, T. Huynh-The, J. I. You, S.-Y. Yu, T. Le-Tien, S.-H. Bae, and S. Lee, "Convolutional network with twofold feature augmentation for diabetic retinopathy recognition from multi-modal images," *IEEE J. Biomed. Health Informat.*, vol. 25, no. 7, pp. 2686–2697, Jul. 2021, doi: 10.1109/JBHI.2020.3041848.

[26] L. Chen, Y. Wei, Z. Yao, E. Chen, and X. Zhang, "Data augmentation in prototypical networks for forest tree species classification using airborne hyperspectral images," *IEEE Trans. Geosci. Remote Sens.*, vol. 60, pp. 1–16, 2022, doi: 10.1109/TGRS.2022.3168054.

[27] J. Liu, C. Shen, N. Aguilera, C. Cukras, R. B. Hufnagel, W. M. Zein, T. Liu, and J. Tam, ''Active cell appearance model induced generative adversarial networks for annotation-efficient cell segmentation and identification on adaptive optics retinal images,'' *IEEE Trans. Med. Imag.*, vol. 40, no. 10, pp. 2820–2831, Oct. 2021, doi: 10.1109/TMI.2021.3055483.

[28] X. Miao, Y. Zhang, J. Zhang, and X. Liang, ''Hierarchical CNN classification of hyperspectral images based on 3-D attention soft augmentation,'' *IEEE J. Sel. Topics Appl. Earth Observ. Remote Sens.*, vol. 15, pp. 4217–4233, 2022, doi: 10.1109/JSTARS.2022.3174301.

[29] J. Meng, W. Hu, L. Jia, G. He, and P. Xue, ''A semantic segmentation model for headdresses in thangka image based on line drawing augmentation and spatial prior knowledge,'' *IEEE Sensors J.*, vol. 21, no. 22, pp. 25161–25170, Nov. 2021, doi: 10.1109/JSEN.2021.3076765.

[30] M. T. Hossain, S. W. Teng, F. Sohel, and G. Lu, ''Robust image classification using a low-pass activation function and DCT augmentation,'' *IEEE Access*, vol. 9, pp. 86460–86474, 2021, doi: 10.1109/ACCESS.2021.3089598.

[31] J. Zhang, M. Xing, G.-C. Sun, and X. Shi, ''Vehicle trace detection in two-pass SAR coherent change detection images with spatial feature enhanced unet and adaptive augmentation,'' *IEEE Trans. Geosci. Remote Sens.*, vol. 60, pp. 1–15, 2022, doi: 10.1109/TGRS.2022.3194903.

[32] T. Kim, H. Kim, and H. Byun, ''Localization-aware adaptive pairwise margin loss for fine-grained image recognition,'' *IEEE Access*, vol. 9, pp. 8786–8796, 2021, doi: 10.1109/ACCESS.2021.3049305.

[33] H. Zhang, Z. Xu, X. Han, and W. Sun, ''Data augmentation using bitplane information recombination model,'' *IEEE Trans. Image Process.*, vol. 31, pp. 3713–3725, 2022, doi: 10.1109/TIP.2022.3175429.

[34] X. Sun, X. Jia, Y. Liang, M. Wang, and X. Chi, ''A defect detection method for a boiler inner wall based on an improved YOLO-v5 network and data augmentation technologies,'' *IEEE Access*, vol. 10, pp. 93845–93853, 2022, doi: 10.1109/ACCESS.2022.3204683.

[35] Q. Guo, J. Zhang, C. Zhong, and Y. Zhang, ''Unsupervised multiple change detection for multispectral images based on AMMF and SpatioSpectral channel augmentation,'' *IEEE Geosci. Remote Sens. Lett.*, vol. 19, pp. 1–5, 2022, doi: 10.1109/LGRS.2021.3074423.

[36] A. Singh and L. Bruzzone, ''SIGAN: Spectral index generative adversarial network for data augmentation in multispectral remote sensing images,'' *IEEE Geosci. Remote Sens. Lett.*, vol. 19, pp. 1–5, 2022, doi: 10.1109/LGRS.2021.3093238.

[37] K. Han, L. Liu, Y. Song, Y. Liu, C. Qiu, Y. Tang, Q. Teng, and Z. Liu, ''An effective semi-supervised approach for liver CT image segmentation,'' *IEEE J. Biomed. Health Informat.*, vol. 26, no. 8, pp. 3999–4007, Aug. 2022, doi: 10.1109/JBHI.2022.3167384.

[38] Y. Jiang, B. Ku, W. Kim, and H. Ko, ''Side-scan sonar image synthesis based on generative adversarial network for images in multiple frequencies,'' *IEEE Geosci. Remote Sens. Lett.*, vol. 18, no. 9, pp. 1505–1509, Sep. 2021, doi: 10.1109/LGRS.2020.3005679.

[39] J.-H. Kim and Y. Hwang, ''GAN-based synthetic data augmentation for infrared small target detection,'' *IEEE Trans. Geosci. Remote Sens.*, vol. 60, pp. 1–12, 2022, doi: 10.1109/TGRS.2022.3179891.

[40] H. Gao, J. Zhang, X. Cao, Z. Chen, Y. Zhang, and C. Li, ''Dynamic data augmentation method for hyperspectral image classification based on Siamese structure,'' *IEEE J. Sel. Topics Appl. Earth Observ. Remote Sens.*, vol. 14, pp. 8063–8076, 2021, doi: 10.1109/JSTARS.2021.3102610.

[41] J. Hu, X. Shen, H. Yu, X. Shang, Q. Guo, and B. Zhang, ''Extended subspace projection upon sample augmentation based on global spatial and local spectral similarity for hyperspectral imagery classification,'' *IEEE J. Sel. Topics Appl. Earth Observ. Remote Sens.*, vol. 14, pp. 8653–8664, 2021, doi: 10.1109/JSTARS.2021.3107105.

[42] X. Xu, B. Zhao, X. Tong, H. Xie, Y. Feng, C. Wang, C. Xiao, X. Ke, and J. Du, ''A data augmentation strategy combining a modified pix2pix model and the copy-paste operator for solid waste detection with remote sensing images,'' *IEEE J. Sel. Topics Appl. Earth Observ. Remote Sens.*, vol. 15, pp. 8484–8491, 2022, doi: 10.1109/JSTARS.2022.3209967.

[43] T. Song, S. Kim, and K. Sohn, ''Shape-robust SAR ship detection via context-preserving augmentation and deep contrastive RoI learning,'' *IEEE Geosci. Remote Sens. Lett.*, vol. 19, pp. 1–5, 2022, doi: 10.1109/LGRS.2022.3190855.

[44] J. Krebs, H. Delingette, N. Ayache, and T. Mansi, ''Learning a generative motion model from image sequences based on a latent motion matrix,'' *IEEE Trans. Med. Imag.*, vol. 40, no. 5, pp. 1405–1416, May 2021, doi: 10.1109/TMI.2021.3056531.

[45] P. Gudžius, O. Kurasova, V. Darulis, and E. Filatovas, ''Deep learning-based object recognition in multispectral satellite imagery for real-time applications,'' *Mach. Vis. Appl.*, vol. 32, no. 4, p. 98, Jul. 2021.

[46] L. Lin, C. Chen, and T. Xu, ''Spatial-spectral hyperspectral image classification based on information measurement and CNN,'' *EURASIP J. Wireless Commun. Netw.*, vol. 2020, no. 1, Dec. 2020, Art. no. 59.

[47] W. Lv and X. Wang, ''Overview of hyperspectral image classification,'' *J. Sensors*, vol. 2020, no. 2, pp. 1–13, 2020.

[48] I. H. Sarker, ''Machine learning: Algorithms, real-world applications and research directions,'' *Social Netw. Comput. Sci.*, vol. 2, no. 3, May 2021, Art. no. 160.

[49] J. Transon, R. d'Andrimont, A. Maugnard, and P. Defourny, ''Survey of hyperspectral earth observation applications from space in the Sentinel-2 context,'' *Remote Sens.*, vol. 10, no. 2, p. 157, 2018.

[50] C. Guo, H. Tang, B. Niu, and C. B. P. Lee, ''A survey of bacterial foraging optimization,'' *Neurocomputing*, vol. 452, pp. 728–746, Sep. 2021.

[51] A. G. Gad, ''Particle swarm optimization algorithm and its applications: A systematic review,'' *Arch. Comput. Methods Eng.*, vol. 29, no. 5, pp. 2531–2561, Aug. 2022.

[52] C. Shorten and T. M. Khoshgoftaar, ''A survey on image data augmentation for deep learning,'' *J. Big Data*, vol. 6, no. 1, pp. 1–48, Dec. 2019.

[53] S. Santra, S. Mandal, K. Das, J. Bhattacharjee, and A. Deyasi, ''A comparative study of Z-transform and Fourier transform applied on medical images for detection of cancer segments,'' in *Proc. 3rd Int. Conf. Electron., Mater. Eng. Nano-Technol. (IEMENTech)*, Aug. 2019, pp. 1–4.

[54] V. Bhavana and H. K. Krishnappa, ''Multi-modality medical image fusion using discrete wavelet transform,'' *Proc. Comput. Sci.*, vol. 70, pp. 625–631, Dec. 2015.

[55] C. Scribano, G. Franchini, M. Prato, and M. Bertogna, ''DCT-former: Efficient self-attention with discrete cosine transform,'' *J. Sci. Comput.*, vol. 94, no. 3, p. 67, Mar. 2023.

[56] I. Stankovic, M. Brajovic, L. Stankovic, and M. Dakovic, ''Laplacian filter in reconstruction of images using gradient-based algorithm,'' in *Proc. 29th Telecommun. Forum (TELFOR)*, Belgrade, Serbia, Nov. 2021, pp. 1–4, doi: 10.1109/TELFOR52709.2021.9653297.

[57] P. R. Dave and H. A. Pandya, ''Satellite image classification with data augmentation and convolutional neural network,'' in *Advances in Electrical and Computer Technologies* (Lecture Notes in Electrical Engineering). Singapore: Springer, 2020, pp. 83–92.

[58] M. A. A. Ghaffar, A. McKinstry, T. Maul, and T. T. Vu, ''Data augmentation approaches for satellite image super-resolution,'' *ISPRS Ann. Photogramm., Remote Sens. Spatial Inf. Sci.*, vol. 4, pp. 47–54, Sep. 2019.

[59] X. Yu, X. Wu, C. Luo, and P. Ren, ''Deep learning in remote sensing scene classification: A data augmentation enhanced convolutional neural network framework,'' *GIScience Remote Sens.*, vol. 54, no. 5, pp. 741–758, May 2017.

[60] I. M. De Diego, A. R. Redondo, R. R. Fernández, J. Navarro, and J. M. Moguerza, ''General performance score for classification problems,'' *Appl. Intell.*, vol. 52, no. 10, pp. 12049–12063, Jan. 2022.

[61] M. A. Kadhim and M. H. Abed, ''Convolutional neural network for satellite image classification,'' in *Intelligent Information and Database Systems: Recent Developments*. Cham, Switzerland: Springer, Mar. 2019, pp. 78–165.

[62] S. Mirjalili, S. M. Mirjalili, and A. Lewis, ''Grey wolf optimizer,'' *Adv. Eng. Softw.*, vol. 69, pp. 46–61, Mar. 2014.

DIPEN SAINI received the M.Tech. degree from GNDU Amritsar. He is currently pursuing the Ph.D. degree with Lovely Professional University (LPU), Punjab. He has expertise in teaching and research and development for five years. His most of research work is in satellite images. His research interests include machine learning, deep learning, and image processing.

RAHUL MALIK received the M.Tech. degree from NIT Nagpur and the Ph.D. degree from NIT, Jalandhar, Punjab, in 2019. He has expertise in teaching and research and development for seven years. He has more than 20 research articles along with book chapters, including more than five articles in SCI-indexed journals. His research interests include machine learning, deep learning, image processing, and soft computing. He has served as a keynote speaker/session chair/reviewer/TPC member/guest editor in the research fields and many more positions in various conferences and journals.

RACHIT GARG (Member, IEEE) is a COS with the School of Computer Science and Engineering, Lovely Professional University (LPU), Punjab, India. LPU is a young university having more than 30,000 young minds in emerging areas of science and technology on a single campus. The university campus exhibits a rich diversity as the academic staff and students from all 29 states of India and more than 30 countries of the world. He has more than 21 years of teaching and administrative experience as the Director and the Principal to various institutions of repute in Lyallpur Khalsa College, Jalandhar; Universal Institute of Engineering and Technology; and the Sri Sai College of Engineering and Technology. He was the Founding Director with the Pyramid College of Business and Technology, where he has taught subjects, such as distributed mobile computing, software engineering, system analysis and design, operating systems, and data mining. He has published more than 60 research papers(s) in reputed international journals and conferences, which are indexed in various international databases. He has supervised many master's and doctorate students in the various phases of the dissertation. He has also edited books and authored book chapters with international and national publishers. His current research interests include distributed systems, checkpointing, fault tolerance, mobile computing, security, data mining, software engineering, information security, information systems, health informatics, and cyber forensics. He is a senior member of many international conferences in association with IEEE and a Life Member of CSI and IAENG. IEEE and SCRS student chapters have been initiated under his guidance. He has organized IEEE conferences (six in series) and chaired special sessions and delivered various technical sessions at the national and international level. He is currently a guest editor of the Talyor and Francis journals. He is working in various capacities as an editor, an associate editor, and a guest editor. He is also a member of the editorial board of many international journals and conferences.

MOHAMMAD KHALID IMAM RAHMANI (Senior Member, IEEE) was born in Patherghatti, Kishanganj, Bihar, India, in 1975. He received the B.Sc. (Engg.) degree in computer engineering from Aligarh Muslim University, India, in 1998, the M.Tech. degree from Maharshi Dayanand University (MDU), Rohtak, in 2010, and the Ph.D. degree in computer science engineering from Mewar University, India, in 2015. From 1999 to 2006, he was a Lecturer with the Maulana Azad College of Engineering and Technology, Patna. From 2006 to 2008, he was a Lecturer and a Senior Lecturer with the Galgotias College of Engineering and Technology, Greater Noida. From 2010 to 2011, he was an Assistant Professor with MVN, Palwal. Currently, he is an Associate Professor with the Department of Computer Science, College of Computing and Informatics, Saudi Electronic University, Riyadh, Saudi Arabia. He has published more than 60 research papers in journals and conferences of international repute, three book chapters, and holds one USA patent and another Australian patent of innovation. His research interests include algorithms, the IoT, cryptography, image retrieval, pattern recognition, machine learning, and deep learning.

MD. EZAZ AHMED received the M.E. degree in computer science and engineering from MDU University, Rohtak, Haryana, India, in 2008, and the Ph.D. degree in computer science from Jodhpur National University, India, in 2013. He was with North Cap University (NCU) formerly known as ITM University Gurgaon Haryana, India, as an Assistant Professor and another rank, from 2002 to 2013. Since 2014, he has been with the Department of Computer Science, College of Computing and Informatics, Saudi Electronic University, as an Assistant Professor. His research interests include data mining, web technology, machine learning, deep learning, data science, and the IoT.

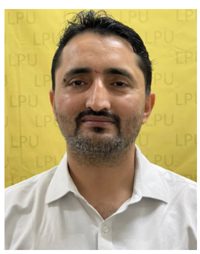

DEEPAK PRASHAR received the B.Tech. degree in computer science and engineering from Punjab Technical University, Punjab, India, in 2007, the M.Tech. degree in computer science and engineering from the PEC University of Technology, Chandigarh, India, in 2009, and the Ph.D. degree from Punjab Technical University. He has been a Professor and the Coordinator of the School of Computer Science and Engineering, Lovely Professional University, Punjab, since 2009. He has published more than 90 research papers in reputed national and international conferences and journals, including SCOPUS and SCIE-indexed journals. His research interests include wireless sensor networks, soft computing, blockchain, machine learning, the IoT, image processing, and cyber security. He is involved in the review process of many SCI or SCIE-indexed journals, such as IEEE, Springer, Wiley, and Inderscience. He is also an editorial board member of recognized journals and serves as a technical program committee member in reputed international conferences in India and abroad.

SUDAN JHA (Senior Member, IEEE) received the bachelor's and master's degrees in engineering from the Motilal Nehru Regional Engineering College (MNREC), Allahabad, India, in 2001 and 2006, respectively, and the Ph.D. degree from MNREC, in 2015. He is the Principal Scientist in the Himalayan Country Nepal. Currently, he is a Professor with the School of Engineering, Kathmandu University, Banepa, Kathmandu, Nepal. He has around 75 accepted and published research papers and book chapters in reputed SCI, SCIE, ESCI, and SCOPUS-indexed journals; and conferences. He has two patents in his name. Additionally, he has authored and edited six books for recent advanced topics in the IoT, 5G, and AI for the publishers, such as Elsevier, CRC, and AAP. He is an internationally acclaimed keynote speaker at several international conferences and a resource person in national/international faculty development programs and the short term training programs for faculties and students. He has served as a guest editor in several SCIE and ESCI journals and a reviewer/TPC member in various conferences and journals. He is the Editor-in-Chief of an international journal published in South Korea.

JABEEN NAZEER received the master's degree in computer applications, in 2001. She is a distinction holder from Osmania University, Hyderabad. She is a Faculty Member with the Department of Computer Science, College of Computer Engineering and Sciences, Prince Sattam Bin Abdulaziz University, Al-Kharj, Saudi Arabia. She has more than 20 years of teaching and research experience. She was the Head of the Department with Princeton College of Engineering until 2006. In 2006, she joined as a Grade H Lecturer with the Higher College of Technology, Muscat, Oman. She has published many research papers in reputed journals and conferences. She has presented her research papers at many national and international conferences. Her research interests include software engineering, big data, data science, and the Internet of Things.

SULTAN AHMAD (Member, IEEE) received the master's degree (Hons.) in computer science and applications from Aligarh Muslim University, India, and the Ph.D. degree from Glocal University. Currently, he is a Faculty Member with the Department of Computer Science, College of Computer Engineering and Sciences, Prince Sattam Bin Abdulaziz University, Al-Kharj, Saudi Arabia. He is also an Adjunct Professor with Chandigarh University, Gharuan, Punjab, India. He has more than 15 years of teaching and research experience. He has around 80 accepted and published research papers and book chapters in reputed SCI, SCIE, ESCI, and SCOPUS-indexed journals and conferences. He has an Australian Patent in his name. He has authored four books that are available on Amazon. He has presented his research papers at many national and international conferences. His research interests include distributed computing, big data, machine learning, and the Internet of Things. He is a member of IACSIT and the Computer Society of India.